First-principles calculations of hyperfine structure in *M*-doped $Si_{16}H_{16}$ fullerene cages (*M*=Cr, Mn, and Fe)

Mohammad Saeed Bahramy,[1,*] Vijay Kumar,[1,2] and Yoshiyuki Kawazoe[1]
[1]*Institute for Materials Research, Tohoku University, Aoba-ku, Sendai 980-8577, Japan*
[2]*Dr. Vijay Kumar Foundation, 1969 Sector 4, Gurgaon, Haryana 122001, India*
(Received 9 April 2009; revised manuscript received 2 June 2009; published 30 June 2009)

We study magnetism and hyperfine structure in $Si_{16}H_{16}$ fullerenes endohedrally doped with a transition-metal atom *M*=Cr, Mn, and Fe using density functional theory calculations. In all cases the endohedral fullerene maintains the same magnetic moment as in a free *M* atom and it is mainly localized on *M* with partial redistribution on the $Si_{16}H_{16}$ cage. However, a comparison between the isotropic hyperfine parameter A_{iso} of *M* dopants with that of free *M* atoms reveals that the electronic wave function at the nucleus of Mn and Fe undergo a significant change both quantitatively and qualitatively as they become doped inside $Si_{16}H_{16}$ cage, while for Cr it remains nearly the same. The endohedral doping of Mn and Fe atoms increases the value of the spin density at the nucleus of the *M* atom, $\rho_s(\mathbf{R}_M)$ and correspondingly, the value of A_{iso}. Analyzing the trend of the core spin-polarization induced by the singly occupied molecular orbitals (SOMOs), it is shown that the increase in the value of A_{iso} for Mn and Fe atoms comes directly from an increase in the contribution of SOMOs to $\rho_s(\mathbf{R}_M)$ and indirectly from hybridization of 3*d* orbitals of the dopants with the *s*- and *p*-like orbitals of the cage. The latter results in a decrease in the spin-polarization of the core 2*s* and 3*s* orbitals so that they less effectively contribute to $\rho_s(\mathbf{R}_M)$. These results are likely to have wider applicability and could offer a way to identify endohedral doping.

DOI: 10.1103/PhysRevB.79.235443 PACS number(s): 73.22.−f, 32.10.Fn, 36.40.Cg, 61.48.−c

I. INTRODUCTION

Recent developments of the stabilization of cage structures of silicon and other group 14 elements by encapsulation of a metal (*M*) atom[1] or by hydrogen termination[2] have led to wide renewed interest in research on silicon nanoparticles.[3] By the encapsulation of an *M* atom, it has been possible to stabilize fullerene and other polyhedral structures of silicon in which *M* atom interacts very strongly with the silicon cage.[1] On the other hand hydrogen termination has been used to stabilize empty cage fullerene structures,[4] which have a large highest occupied molecular orbital-lowest unoccupied molecular orbital (HOMO-LUMO) gap. Such empty cage structures can further be doped with an atom to have endohedral hydrogen-terminated silicon fullerenes. The HOMO-LUMO gap of such silicon fullerenes can be varied by changing the dopant atom, leading to a possibility of a variety of applications. The interaction of the dopant atom with the cage has been shown[4] to be much weaker as compared to the *M* encapsulated silicon clusters and therefore in most cases the dopant atom keeps its atomic character. Accordingly it is possible to dope these cages with magnetic atoms such as Cr, Mn, and Fe to develop silicon fullerene species with large magnetic moments. The aim of this paper is to understand the electronic structure of such magnetic endohedral hydrogenated silicon fullerenes and to suggest nuclear hyperfine structure to be a way to detect endohedral doping as well as their characteristic properties.

Empty-cage hydrogenated silicon fullerenes Si_nH_n (*n* =12, 14, 16, and 20) have been shown[4] to have large HOMO-LUMO gaps of about 3 eV within the density functional theory (DFT) using generalized gradient approximation (GGA) for the exchange-correlation (XC) energy. This large gap makes the overlap of the completely filled orbitals of the dopant atom with those of the cage less favorable due to Pauli repulsion and it is also the reason for the weak doping energies. On the other hand dopants with partially occupied atomic orbitals can have significant overlap with the cage orbitals. Accordingly the changes in the orbitals of the dopant atom due to the surrounding cage could be significant enough to effect the electronic charge density at the nucleus, which in turn would affect the nuclear hyperfine structure leading to a possibility of detecting encapsulation of magnetic dopants. We consider here an intermediate size of the hydrogenated silicon fullerene with *n*=16 and study its endohedral doping with *M*=Cr, Mn, and Fe. These three *M* atoms are interesting as they have high magnetic moments. Also Cr and Mn have half-filled 3*d* shell but different occupations of the 4*s* orbital. On the other hand in the case of Mn and Fe atoms, 4*s* orbital is fully occupied but 3*d* orbitals have different occupancies. Therefore, such a study could lead to an understanding of the effects on the interaction as well as hyperfine structure of the dopant due to varying numbers of *s* and *d* electrons.

II. COMPUTATIONAL METHOD

The atomic structures of the empty cage as well as endohedral hydrogenated silicon fullerenes were studied earlier[4] using VASP code[5] with ultrasoft (U.S.) pseudopotentials and plane-wave (PW) basis set. Here we reoptimize the geometries of the structures self-consistently using the unrestricted Kohn-Sham equations with the B3LYP (Refs. 6 and 7) XC functional and the Gaussian-type 6-311G(*d*) basis set, as implemented in the GAUSSIAN 03 program.[8] The (*d*) sign of the basis set indicates that one *d*-polarization function for Si and one *f*-polarization function for *M* dopants are added to

 ©2009 The American Physical Society

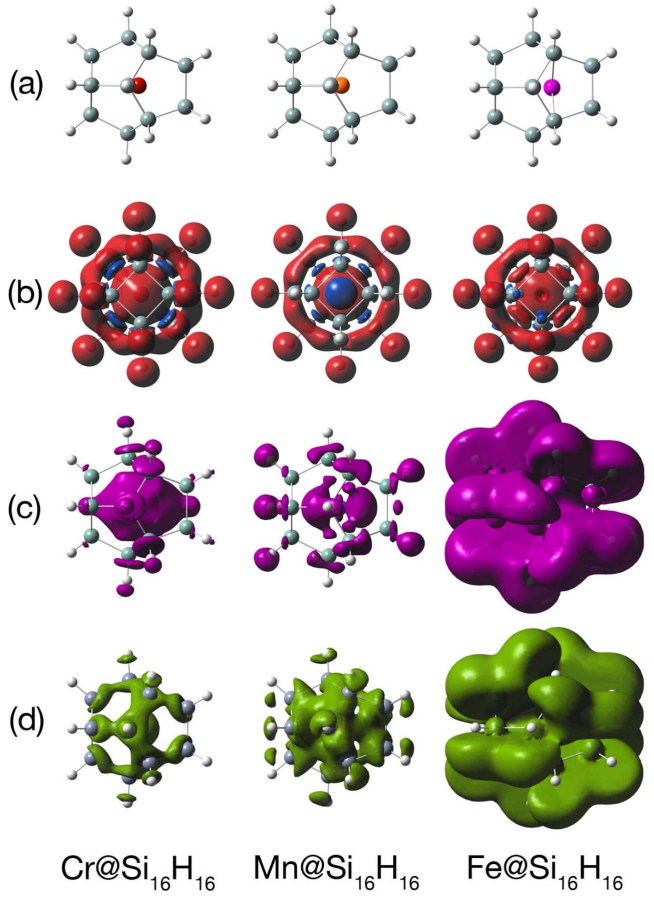

FIG. 1. (Color online) (a) Side view of $M@Si_{16}H_{16}$ structures. The small white and large gray balls represent Si and H atoms of the cage, respectively, whereas the endohedrally encapsulated Cr, Mn, and Fe atoms can be distinguished, respectively, as red, orange, and purple balls (dark balls in gray scale), located inside the $Si_{16}H_{16}$ fullerene cage. (b) Spin density isosurfaces at $\rho_s=0.004$ a.u. as seen from top of $M@Si_{16}H_{16}$ endohedral fullerene along the 4-fold symmetry axis. (c) and (d) show, respectively, the isosurfaces for the excess of charge and the depletion of charge at $\rho=0.0004$ a.u. in $M@Si_{16}H_{16}$ compared with empty cage $Si_{16}H_{16}$ fullerene and isolated M atom at the same positions as in the endohedral fullerene.

the 6–311G basis set.[9] The structures are fully optimized without any constraint on symmetry. The changes in the structures of the empty and the endohedrally doped silicon fullerenes due to the use of B3LYP XC functional and 6-311G(d) basis set are quite small compared with the PW91 (Ref. 10) functional and PW basis set with U.S. pseudopotentials (Ref. 4). The empty fullerene cage consists of 16 silicon atoms located at the corners of eight pentagonal (Si5) and two tetragonal (Si4) faces. Each Si atom is additionally bounded to one H atom [see Fig. 1(a)]. For M=Cr and Mn, the dopant atom is found to be at the center of the $Si_{16}H_{16}$ cage. For Cr (Mn), the nearest neighbor Si4-Si4, Si4-Si5, and Si5-Si5 as well as Si4-M, and Si5-M bond lengths are 2.440 (2.428), 2.423 (2.414), 2.549 (2.463), 3.260 (3.245), and 2.870 Å (2.871 Å), respectively, whereas in the case of M =Fe, the dopant atom drifts slightly toward a pentagon of the cage with nearest-neighbor Si-Si and Si-Fe bond lengths varying from 2.412 and 2.807 Å to 2.454 and 3.41 Å, respectively.

By definition, the isotropic hyperfine parameter A_{iso} is computed from,

$$A_{iso}(M) = \frac{2}{3}\mu_0 g_e \mu_e g_I \mu_I \rho_s(\mathbf{R}_M), \quad (1)$$

where $\rho_s(\mathbf{R}_M)$ is the spin density at the position of the M nucleus $\mathbf{R}_M$ and μ_0 is the permeability of vacuum ($4\pi \times 10^{-7}$ T^2 m^3 J^{-1}). g_e is the electron g factor and μ_e, the Bohr magneton while g_I and μ_I are the gyromagnetic ratio and the magnetic moment of the nucleus, respectively.

After the optimization of the structures, the magnetic moments, A_{iso}, and other related properties are calculated and examined for the M dopant using five different XC functionals, denoted as BLYP, PBEPBE, B3LYP, PBE1PBE, and τ-HCTH.[6,7,11–14] For these density functional methods, the correlation functional is from either Lee, Yang, and Parr (LYP)[7] or Perdew, Burke, and Ernzerhof (PBE),[12,13] while the exchange part is estimated by either Becke's pure DFT (B)[11] and his three-parameter hybrid (B3)[6] exchange functionals or PBE's pure DFT and their respective hybrid (PBE1) exchange functionals.[12,13] τ-HCTH is a highly accurate XC functional belonging to Handy's family functionals.[14]

Throughout this work we do not consider the relativistic effects, e.g., the spin-orbit coupling. As a result, the magnetic moments provided in this study reflect the spin-only values. The local magnetic moments correspond to the Mulliken spin densities computed with the GAUSSIAN 03 program.

As regards the accuracy of the 6-311G(d) basis set for the calculation of A_{iso}, for free M atoms it is examined against the Wachters basis set with a f function,[15,16] the Ahlrichs double ζ basis set with a p-polarization function,[17] and the triple-valence ζ quality basis set plus polarization function by Camiletti and co-workers,[18,19] denoted as Wachters+f, DZP, and TZP, respectively.

III. RESULTS AND DISCUSSIONS

As discussed previously in Ref. 4, endohedrally doped transition M atoms in a $Si_{16}H_{16}$ fullerene cage represent a very interesting local magnetic system. In the cases where the dopant is Cr, Mn, and Fe atom, our calculations predict large total magnetic moments of $6\mu_B$, $5\mu_B$, and $4\mu_B$, respectively. Interestingly, the respective values of the total magnetic moments for these endohedral fullerenes are equal to those of free Cr($4s^13d^5$), Mn($4s^23d^5$), and Fe($4s^23d^6$) atoms as also shown earlier in Ref. 4. Such large magnetic moments turn out to be strongly dominated by the M dopant. According to Table I, the M dopant maintains large local magnetic moments. As a general trend, the pure DFT XC functionals BLYP and PBEPBE tend to underestimate the local moment values by up to $0.19\mu_B$ for Cr, $0.10\mu_B$ for Mn, and $0.13\mu_B$ for Fe, as compared to the other XC functionals.

To demonstrate the magnetic behavior of $M@Si_{16}H_{16}$ fullerenes, we have shown in Fig. 1(b) the spin-density distribution for each cluster at $\rho_s=0.004$ a.u.. The figure clearly indicates that the spin density is substantially localized on

TABLE I. Comparison of the magnetic moments (μ_B) of M dopant inside $Si_{16}H_{16}$ fullerene cage as computed with different XC functionals.

XC	Cr	Mn	Fe
BLYP	5.03	4.49	3.54
PBEPBE	5.02	4.52	3.55
B3LYP	5.18	4.58	3.62
PBE1PBE	5.20	4.55	3.65
τ-HCTH	5.21	4.59	3.67

the M dopant while the rest of the polarization is distributed on the cage, especially on the eight Si atoms that form a ring in the cage and the eight H atoms which are commonly shared between the eight Si pentagons of the cage.

In order to find out the rearrangement of the electronic charge on the cage due to M doping, we have shown in Figs. 1(c) and 1(d) the difference between the charge densities of the endohedral cage and the $Si_{16}H_{16}$ empty cage plus the isolated M atom at the same positions as in the endohedral cage. It is seen that for $Cr@Si_{16}H_{16}$ there is an excess of charge mainly inside of the cage, while for $Mn@Si_{16}H_{16}$ it is also distributed on all the Si atoms as well as the eight H atoms connected to the two squares of silicon cage. In the case of $Fe@Si_{16}H_{16}$, the excess and depletion charges are equally large both inside and outside of the cage. For M =Cr and Mn, there is a depletion of charge near the σ bonds between Si nearest neighbors and around each Si atom, respectively, toward inside the cage. The excess charge around the dopant atom shows a dip below the Si-Si bonds and around each Si atom while some charge bulges out around the center of the faces specially for M=Cr. Such features of the polarization of charge specially for M=Cr arise due to the Pauli exclusion principle because of the close shell repulsion of half-filled $3d$ and $4s$ levels of Cr with the cage as the exchange-splitting is large. Note that for Cr and Mn atoms, the energy to embed in the hydrogenated silicon fullerene cage was shown[4] to be small ($\approx$0.5 eV) while for M=Fe, the energy to embed increases and in this case one can see significant hybridization between the M and the cage orbitals. For Mn, while the bonding with the cage remains weak due to closed $4s$ shell as well as half-filled $3d$ level, there is more hybridization with the cage than for Cr and it is related to the position of the atomic $3d$ and $4s$ levels of Mn as it would be discussed later. For Fe, the hybridization with the cage becomes stronger due to the partially occupied levels as well as due to the overlap of the atomic electronic levels with those of the cage (see below).

TABLE II. Basis set dependence of the isotropic hyperfine parameter A_{iso} (MHz) in $M=^{53}Cr$, ^{55}Mn, and ^{57}Fe. All the values have been calculated using B3LYP functional. The experimental data, Expt., for ^{53}Cr, ^{55}Mn, and ^{57}Fe are taken from Refs. 23–25, respectively.

Basis set	^{53}Cr	^{55}Mn	^{57}Fe
6-311G(d)	−84.36	−28.63	−4.47
Wachters+f	−104.92	−23.98	−3.86
DZP	−97.00	−38.73	−5.51
TZP	−95.99	−14.05	2.25
Expt.	−82.60	−72.40	−10.19

The localization of large magnetic moments on the M dopants implies that the spin density should have a net contribution at the position of the M nucleus that is likely to be comparable to that obtained for the corresponding free M atoms, but modified due to the polarization or hybridization with the cage. Thus, a detailed comparison between A_{iso} of the M dopants with that of free M atoms is expected to reveal valuable information about the nature of bonding and hybridization between M and the $Si_{16}H_{16}$ cage. However, prior to any further calculation, we must first make sure that our basis set is sufficiently accurate to treat the wave function and correspondingly the spin density at the M nucleus. On this basis, using B3LYP functional we have performed a set of test calculations on free M atoms to evaluate the accuracy of 6-311G(d) basis set against three other basis sets, namely, Wachters+f, DZP, and TZP. Table II summarizes the respective A_{iso} values computed with these basis sets as well as the corresponding experimental data. The table clearly indicates that within nonrelativistic B3LYP approximation, the 6-311G(d) basis set gives reasonable A_{iso} for M atoms which are first of all in good agreement with the experimental values and moreover compare well with those obtained from the other basis sets. All the four basis sets commonly show the largest error in A_{iso} for Mn and Fe. However, below we show that changing the XC functional to τ-HCTH, the error will be substantially corrected. On this basis, the 6-311G(d) basis set is expected to be a good choice to com-

TABLE III. Comparison of the isotropic hyperfine parameters A_{iso} (MHz) for Cr, Mn, and Fe considered as free atoms and as dopants inside a $Si_{16}H_{16}$ fullerene cage.

Atom	BLYP	PBEPBE	B3LYP	PBE1PBE	τ-HCTH	Expt.[a]
^{53}Cr	−92.10	−80.90	−84.36	−71.13	−88.17	−82.60
^{55}Mn	−7.96	−16.27	−28.63	−38.79	−81.48	−72.40
^{57}Fe	5.00	9.13	−4.47	−5.78	−10.06	−10.19
$^{53}Cr@Si_{16}H_{16}$	−83.60	−72.82	−82.92	−71.60	−72.78	
$^{55}Mn@Si_{16}H_{16}$	184.64	125.14	515.25	448.98	119.165	
$^{57}Fe@Si_{16}H_{16}$	83.67	73.32	88.02	78.18	77.36	

[a]see Table II.

TABLE IV. Spin densities at the M nucleus $\rho_s(\mathbf{R}_M)$ (a.u.) and isotropic hyperfine parameters A_{iso} (MHz) for Cr, Mn, and Fe considered as free atoms and as dopants inside a $Si_{16}H_{16}$ fullerene cage using τ-HCTH functional. VS refers to the valence states other than the singly occupied molecular orbital (SOMO).

	Contributions							
	Core							
Atom	1s	2s	3s	VS	SOMO	Total	Expt.[a]	3s/2s
^{53}Cr	0.03	−2.46	1.19	0.00	3.33	2.09	1.96	−0.48
^{55}Mn	0.01	−3.09	1.52	1.19	0.00	−0.37	−0.35	−0.49
^{57}Fe	0.00	−2.69	1.31	1.06	0.00	−0.32	−0.28	−0.49
^{53}Cr @ $Si_{16}H_{16}$	0.03	−2.28	1.09	0.46	2.42	1.72		−0.48
^{55}Mn @ $Si_{16}H_{16}$	0.01	−2.69	1.33	−1.01	2.90	0.54		−0.49
^{57}Fe @ $Si_{16}H_{16}$	0.01	−1.94	0.97	0.31	2.78	2.13		−0.50

[a]Experimental values for $\rho_s(\mathbf{R}_M)$ were obtained from Eq. (1) using the respective experimental $A_{iso}(M)$ data noted in Table II.

promise the required accuracy for the hyperfine calculations with the computational limitations.

Having confirmed the reliability of the basis set, our calculations reveal that except for Cr, the A_{iso} values of M dopants undergo a significant change as they become doped inside $Si_{16}H_{16}$ cage (see Table III). According to Table III, the absolute values of A_{iso} for Mn and Fe dopants are much larger than those obtained for free Mn and Fe atoms, respectively. Additionally, the A_{iso} values corresponding to these dopants are positive in contrast to the negative values for the free Mn and Fe atoms. The above changes indicate that, for M atoms doped inside $Si_{16}H_{16}$ cage, $\rho_s(\mathbf{R}_M)$ should be substantially dominated by the wave functions of spin-up electrons.

It is to be noted that the spin density at the M nucleus originates both directly and indirectly from the singly occupied molecular orbitals (SOMOs). The former happens if SOMO is purely s-like (4s for M) whereas the non-s-like SOMOs contribute indirectly to the spin density at the M nucleus by spin-polarizing the inner core and paired valence states (VS) s-shells. It is worth mentioning that for M elements VS contributions originate from the spin-polarization of valence 4s states, also. We have calculated the core, VS, and SOMO contributions to $\rho_s(\mathbf{R}_M)$ for M atoms doped in $Si_{16}H_{16}$ cage as well as for free atoms by using τ-HCTH functional. This functional has been chosen as it excellently reproduces the experimental A_{iso} values for free M atoms (see Table III). The other functionals are less accurate and for Mn and Fe they tend to overestimate the experimental hyperfine data.

As shown in Table IV, there is a striking similarity between the trend of the core spin-polarization (CSP) in free M atoms and that in M doped inside $Si_{16}H_{16}$ cage. In both the cases, 1s orbital has almost no impact on $\rho_s(\mathbf{R}_M)$ while 2s and 3s orbitals contribute significantly to $\rho_s(\mathbf{R}_M)$, *albeit* with opposite signs. The former always has negative sign while the latter is positive in all cases with a smaller absolute value compared with the 2s contribution. More interestingly, the ratio between 3s and 2s contributions, denoted as 3s/2s ratio in Table IV, for all M atoms remains close to −0.50 even after doping. It is worth to note that Munzárova *et al.* have

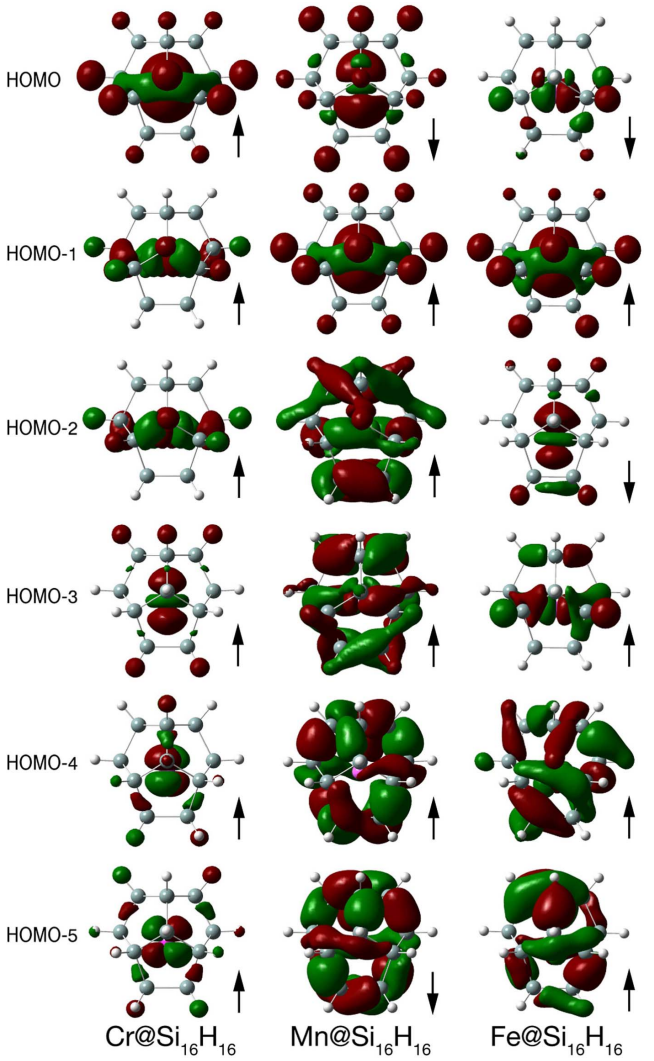

FIG. 2. (Color online) Electronic wave function distributions of the HOMO and the corresponding five molecular orbitals below the HOMO, denoted as HOMO-1 to HOMO-5 calculated for M @ $Si_{16}H_{16}$ fullerene cages using τ-HCTH functional.

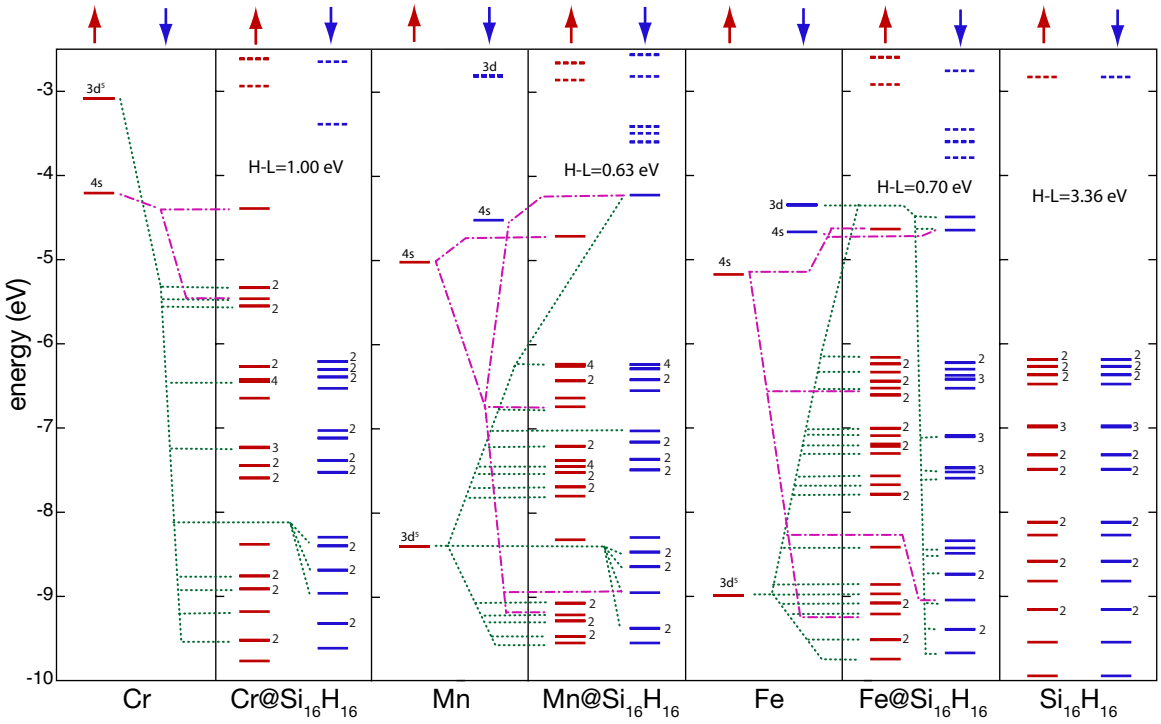

FIG. 3. (Color online) Calculated one-electron energy levels for free M atoms, $M@Si_{16}H_{16}$ fullerenes, and the empty $Si_{16}H_{16}$ cage. The discrete solid and dashed lines correspond to the occupied and unoccupied energy states. The dash-dotted (purple) and dotted (green) lines either indicate the energy levels of $M@Si_{16}H_{16}$ that have strong hybridization with 4s and 3d states of the M dopant, respectively, or show levels that are substantially dominated by respective 4s and 3d states of the M atom. H-L stands for the energy gap between HOMO and LUMO.

found the same $3s/2s$ ratios for other transition M complexes.[20] In their comprehensive study, they found that such a trend of CSP drives from the exchange interaction of inner core and valence shells with SOMOs.[20–22] The similarity between $3s/2s$ ratios was further attributed to the required orthogonality between 2s and 3s orbitals. Apart from this similarity, one can clearly notice a reduction in 2s and 3s contributions to $\rho_s(\mathbf{R}_M)$ as M atom becomes encapsulated inside $Si_{16}H_{16}$ cage and in the case of Fe, the reduction is more significant. On the other hand, the total valence contribution (VS+SOMO) to $\rho_s(\mathbf{R}_M)$ dominantly increases for Mn and Fe. As a result, the total $\rho_s(\mathbf{R}_M)$ on M dopants becomes larger than that on free M atoms.

The above changes can be attributed to two main changes in the characteristics of the SOMOs. The first and the most evident change is that for all M dopants in the fullerene cage, 4s orbital contributes significantly to SOMOs, whereas they are purely 3d-like in the case of free Mn and Fe atoms (see VS and SOMO contributions in Table IV). This can be clearly seen in Fig. 2 where we have demonstrated HOMO and the corresponding five molecular orbitals below HOMO, denoted as HOMO-1 to HOMO-5 for $M@Si_{16}H_{16}$. The figure clearly shows a striking similarity between HOMO of $Cr@Si_{16}H_{16}$ and HOMO-1 of the other two fullerenes. For all these states, the wave functions are strongly localized on M and partially on the H atoms as well as some Si-Si bonds. The spherical shape of the wave functions represents the s character of these singly occupied molecular states. As a direct result, the corresponding SOMOs dominate $\rho_s(\mathbf{R}_M)$ on all the M dopants.

The second change is related to the CSP reduction. As we mentioned earlier, CSP is induced via the exchange interaction of SOMOs with the inner core levels. For transition M atoms, such an interaction can substantially split and, hence, spin-polarize the core levels if the SOMOs are mainly 3d-like, while the SOMOs with 4s character have very negligible effect on the splitting of the inner states. On this basis, we expect that by doping, the SOMOs partially lose their 3d character so that the M dopants experience less pronounced CSP than the free M atoms. To be more correct, the loss of the SOMOs 3d character is due to the hybridization of the 3d states of the M dopants with the s and p states of the cage. In going from Cr to Fe, our calculations reveal a considerable increase in the spd hybridization between the cage and the dopant inside. According to Fig. 2, in $Cr@Si_{16}H_{16}$, almost all the five states below HOMO retain their 3d-like distributions around Cr. The only exceptions are the doubly degenerated states HOMO-1 and HOMO-2 in which one can notice a small charge sharing between the cage and Cr atom. For the other two clusters, the HOMO is mainly 3d-like with a small mixture from 4s, while HOMO-2 (HOMO-3) to HOMO-5 corresponding to $Mn@Si_{16}H_{16}$ ($Fe@Si_{16}H_{16}$) represent hybrid molecular orbitals distributed over the cage as well as the dopant.

To better understand the picture of the hybridization between M and $Si_{16}H_{16}$ fullerene cage, we have demonstrated in Fig. 3 the respective one-electron energy levels calculated for free M atoms, $M@Si_{16}H_{16}$ endohedral fullerenes, and the parent $Si_{16}H_{16}$ fullerene cage. Comparing the positions of $M@Si_{16}H_{16}$ energy levels to those obtained for M and

$Si_{16}H_{16}$ cage, the energy levels of the doped cages can be divided into two groups. The first group corresponds to those occupied states located in between the HOMO and the LUMO of $Si_{16}H_{16}$. All the remaining states below the HOMO of $Si_{16}H_{16}$ constitute the second group. The former can be characterized as nearly *M*-like states as they substantially maintain the 4*s* and 3*d* characters of *M*. The latter are accordingly attributed to the cage's states, *albeit*, partially mixed up and hybridized with *M* states. As a main characteristic, this group of states approximately conform with the energy levels of the empty cage within the same energy range. However, due to interaction with *M*, many of the initially degenerated states of the cage have been distorted and partially spin-polarized.

Figure 3 further reveals that Cr doped inside $Si_{16}H_{16}$ has the weakest interaction with the cage, while the other *M* dopants, especially Fe, effectively interact with $Si_{16}H_{16}$ and hence, exhibit a very rich picture of hybridization. As can be seen in Fig. 3, 4*s* and 3*d* states of Cr are energetically far above the HOMO of $Si_{16}H_{16}$. Accordingly, there's little chance for these orbitals to be hybridized with *s*- and *p*-like orbitals of the cage. As a result, with a large energy difference, they lie above the other states, somewhere inside the HOMO-LUMO gap of the parent $Si_{16}H_{16}$ cage. Such a weak interaction describes why A_{iso} of Cr doped inside $Si_{16}H_{16}$ does not differ much from that obtained for a free Cr atom.

Contrary to Cr, Mn and Fe behave differently when encapsulated inside the $Si_{16}H_{16}$ cage. As shown in Fig. 3, the electron-rich 3*d* states of these atoms lie in an energy range where they can ideally interact with cage states. This leads to a very significant *spd* hybridization between the *M* and the cage orbitals. The 4*s* orbital of the dopant is less affected, as energetically it lies far above the other states. However, in the spin-down channel, 4*s* state becomes partially mixed up with the 3*d* states, mainly $3d_{z^2}$, and partly shared with the cage. Such an orbital admixture is mainly due to the symmetry constraints imposed by the cage. Within the space confined by the D_{4d} symmetry of the cage, both the atomic 4*s* and 3*d* orbitals of *M* undergo a deformation lowering their initial symmetries. Consequently, 4*s* and $3d_{z^2}$ transform to the same state A_{1g}.[26] Thus, they can be mixed up together if they are energetically close enough to each other as it can be seen in the spin-down channel of Fe and Mn. Due to this change, on both Mn and Fe dopants electrons with 4*s* character are more localized in spin-up channel than in spin-down one and, hence, they more effectively contribute to $\rho_s(\mathbf{R}_M)$. The above points explain why such a sharp increase happens to the SOMO contributions for Mn and Fe to $\rho_s(\mathbf{R}_M)$ as they become doped inside $Si_{16}H_{16}$ cage (see Table IV).

IV. SUMMARY

In summary we have studied the magnetic behavior of $Si_{16}H_{16}$ silicon fullerene cages endohedrally doped with Cr, Mn, and Fe atoms. Such species are found to have the same magnetic moments as the free transition-metal dopant atoms and therefore they offer interesting possibilities for applications at subnanomater scale. However, the endohedral doping leads to significant changes in the nucleus hyperfine parameter which can be used to detect endohedral doping. We expect similar results for other silicon fullerene cages. Also such effects on hyperfine structure can be generally expected in other similar systems. It is hoped that our studies would further stimulate experiments on fullerenes of silicon and their realization in the near future similar to the endohedral carbon fullerenes.

ACKNOWLEDGMENTS

M.S.B would like to thank R. V. Belosludov and F. Pichierri for helpful discussions. He also gratefully acknowledges the financial support provided by the Japan Society for the Promotion of Science. V.K. gratefully acknowledges the hospitality at the International Frontier Center for Advanced Materials of IMR and the support of M. W. Chen as well as partial support from the U.S. Asia Office of Aerospace Research and Development. The authors thank the staff of the Centre for Computational Materials Science at the IMR for the use of the Hitachi SR11000 (Model K-2) supercomputer system.

*saeed@imr.edu

[1] V. Kumar and Y. Kawazoe, Phys. Rev. Lett. **87**, 045503 (2001); **91**, 199901 (2003); V. Kumar, Comput. Mater. Sci. **36**, 1 (2006).
[2] V. Kumar and Y. Kawazoe, Phys. Rev. Lett. **90**, 055502 (2003).
[3] V. Kumar, in *Nanosilicon*, edited by V. Kumar (Elsevier, Oxford, 2008).
[4] V. Kumar and Y. Kawazoe, Phys. Rev. B **75**, 155425 (2007).
[5] Vienna *Ab initio* Software Packages (VASP), version 4.6.12 (http://cms.mpi.univie.ac.at/vasp/).
[6] A. D. Becke, J. Chem. Phys. **98**, 5648 (1993).
[7] C. Lee, W. Yang, and R. G. Parr, Phys. Rev. B **37**, 785 (1988).
[8] M. J. Frisch *et al.*, GAUSSIAN 03 program, Revision D.01, Gaussian, Inc., Wallingford CT, 2004.
[9] Æ. Frisch, M. J. Frisch, and G. W. Trucks, *Gaussian 03 User's Reference, Version 7.0* (Gaussian Inc., Cornegie Office Park, 2003), p. 26.
[10] J. P. Perdew and Y. Wang, Phys. Rev. B **45**, 13244 (1992).
[11] A. D. Becke, Phys. Rev. A **38**, 3098 (1988).
[12] J. P. Perdew, K. Burke, and M. Ernzerhof, Phys. Rev. Lett. **77**, 3865 (1996).
[13] J. P. Perdew, K. Burke, and M. Ernzerhof, Phys. Rev. Lett. **78**, 1396 (1997).
[14] A. D. Boese and N. C. Handy, J. Chem. Phys. **116**, 9559 (2002).
[15] A. J. H. Wachters, J. Chem. Phys. **52**, 1033 (1970).
[16] C. W. Bauschlicher, Jr., S. R. Langhoff, H. Partridge, and L. A. Barnes, J. Chem. Phys. **91**, 2399 (1989).
[17] A. Schafer, H. Horn, and R. Ahlrichs, J. Chem. Phys. **97**, 2571 (1992).

[18] G. G. Camiletti, A. Canal Neto, S. F. Machado, and F. E. Jorge, (unpublished).
[19] The TZP basis sets can be freely downloaded at http://www.cce.ufes.br/qcgv/pub/.
[20] M. L. Munzarová, P. Kubáčhek, and M. Kaupp, J. Am. Chem. Soc. **122**, 11900 (2000).
[21] M. L. Munzarová and M. Kaupp, J. Phys. Chem. A **103**, 9966 (1999).
[22] M. S. Bahramy, M. H. F. Sluiter, and Y. Kawazoe, Phys. Rev. B **73**, 045111 (2006).
[23] W. J. Childs, L. S. Goodman, and D. von Ehrenstein, Phys. Rev. **132**, 2128 (1963).
[24] S. J. Davis, J. J. Wright, and L. C. Balling, Phys. Rev. A **3**, 1220 (1971).
[25] W. J. Childs, Phys. Rev. **160**, 9 (1967).
[26] P. W. Atkins and R. S. Friedman, *Molecular Quantum Mechanics*, 3rd ed. (Oxford University Press, New York, 2003), p. 525.